MICROFABRICATION OF HYDROGEL SUBSTRATES OF TUNABLE YOUNG'S MODULUS

A Thesis

Presented to the Faculty of the Graduate School

of Cornell University

in Partial Fulfillment of the Requirements for the Degree of

Master of Science

by

Jonathan Marc Charest

January 2012

ABSTRACT

Much is known about the effects of matrix stiffness and matrix topography on cell behavior, however they are seldom investigated in tandem. Presented and validated here is a micromolding method to introduce topographical features onto polyacrylamide (PA) substrates of tunable Young's modulus (E). Feature fidelity is largely influenced by hydrogel swelling and most efficient on gels with a crosslinker concentration above 4.5%. However, this swelling does not affect the spacing of surface patterned ligands on two-dimensional PA gels. Bovine aortic endothelial cells (BAECs) cultured on linear micromolded features exhibit greater degrees of contact guidance with greater substrate E. Also described are applications of micromolding for future studies in cell mechanics.

BIOGRAPHICAL SKETCH

Jonathan Charest received his B.S. in Biomedical Engineering from Worcester Polytechnic Institute in 2009 prior to pursuing graduate study at Cornell University.

ACKNOWLEDGEMENTS

The publication based on this work [1] in the journal *Macromolecular Bioscience* would not have been possible without the contributions of Joseph P. Califano and Shawn P. Carey. Joe characterized the E values of several commonly used gel formulations in the lab and carried out much of the work on surface-patterned ligand spacing. Shawn provided much aid in acquiring confocal fluorescent images used in our publication [1]. Aside from these specifics, I'd like to acknowledge my peers in the Reinhart-King laboratory for their phenomenal support and camaraderie. Also, the Morgan Family for their financial support.

TABLE OF CONTENTS

LIST OF TABLES

LIST OF FIGURES

CHAPTER 1

INTRODUCTION

1.1 Background

Current research has brought much attention to the role of microenvironmental cues in determining cell behavior [3]. *In vivo* , these cues promote the maintenance of homeostasis in healthy tissues. Changes in both these cues and their interpretation by cells can lead to the development of disease states. Understanding the mechanisms by which cells integrate microenvironmental cues may aid in the development of future medical technologies, specifically in tissue engineering.

The ability of cells to sense their surrounding mechanical environment is derived from the cytoskeleton and its integration with countless signal transduction pathways. A cell's cytoskeleton—made up of filamentous actin, microtubules, and intermediate filaments—is connected to the microenvironment through transmembrane proteins that bind extracellular moieties. Integrins connect the cytoskeleton to the surrounding extracellular matrix (ECM), while cadherins, selectins and immunoglobulins mediate cell-cell connections. Associated with cell-matrix and cell-cell adhesions are a slew of signaling molecules including, but certainly not limited to, focal adhesion kinase (FAK), extracellular-signal-regulated kinases (ERKs), and Src. Downstream of these adhesions are GTPases such as RhoA, Rac1, and Cdc42, responsible for activating or deactivating other programs of cell activity such as contractility, spreading, and process extension. There is a complex network through which mechanical signals are integrated into cell behavior decisions. Consequently, small pertur-

bations of input signals can cause disruption of proper signal integration, leading to disease.

Angiogenesis, the process of new blood vessel formation from existing vessels, is a crucial component of development, wound healing, and pathogenesis. For example, in cancer, angiogenesis enables the formation of vasculature within tumors. However this tumor vasculature is often disorganized and leaky, indicative of dysregulated angiogenesis [4]. Dysregulated angiogenesis has also been implicated in many other diseases such as diabetes, atherosclerosis, inflammatory bowel disease, and hypertension [4]. Key to this dysregulation is aberrant cellular responses to endothelial morphogenic regulators which include soluble [5] and mechanical cues [6]. Normal angiogenesis starts with the breakdown of ECM in the basement membrane. This can be initiated by molecules such as fibroblast growth factor (FGF) [7] or other cues. The resulting changes in the mechanical properties of the matrix induce neighboring endothelial cells to sprout or invade into the surrounding matrix to form nascent tubules that eventually mature into vessels [6]. When cells cannot properly integrate the normal cues that guide angiogenesis or when faulty cues are present, disorganized and immature vasculature or even vessel regression can result [6, 4, 5]. Angiogenesis therefore requires precise regulation *in vivo*.

The disruption of mechanical microenvironmental cues and their integration can be found in numerous disease contexts such as atherosclerosis [3], cancer metastasis [8], progeria, and muscular dystrophy [9] for example. Understanding how cells interpret cues from their mechanical microenvironments is crucial to advancing disease treatment and tissue engineering.

1.2 Matrix stiffness and topography influence cell behavior

1.2.1 Substrate stiffness

The mechanical stiffness of the extracellular matrix (ECM) is known to influence both cell and tissue behavior. Matrix mechanical properties vary across both length scale and tissue type [10]. For example, brain tissue stiffness is around 1 kPa while bone has a modulus on the order of gigapascals. As such, cell types native to different tissues exposed to identical sets of mechanical cues *in vitro* can exhibit differing degrees of response to those cues [11, 10]. Changes in the local matrix stiffness can cause changes in cellular function. *In vivo*, tumors are one example where tissue stiffness is can be altered. Such alterations in matrix stiffness elicit changes in cellular behavior by disrupting cellular mechanical homeostasis [8].

Any alterations in the cellular machinery used to sense the mechanical properties of the microenvironment can result in aberrant behavior. To date, *in vitro* experimentation systems for studying the effects of matrix stiffness traditionally utilize flat cell culture substrates with a variable Young's modulus (E). By far, the most common cell culture substrates used when exploring the effects of stiffness on cell behavior are polyacrylamide (PA) gels. This is due to the ease of tuning the Young's modulus of the gel through its composition. Unmodified, the PA gel surface is non-adhesive to cells. Several methods exist for the addition of adhesive ligands to its surface, making its surface chemistry highly controllable. Despite its advantages, PA gels serve primarily as two-dimensional substrates. Mechanobiology studies seeking to explore cell behavior in three dimensions usually employ hydrogels composed of biological polymers such

as collagen or fibrin. Using such two-dimensional substrates, stiffness has been shown to influence many aspects of cellular behavior.

In 1997, Pelham and Wang were the first to show that cells can sense the stiffness of the culture substrate. Their data illustrated that normal rat kidney epithelial cells migrate slower on stiff substrates and that substrate stiffness influences the morphology of adhesions structures [12]. Later work by Lo *et al*. suggested that fibroblasts preferentially migrate to areas of greater stiffness and exert greater traction forces on the substrate [13]. This influence on cell migration was also shown to occur with smooth muscle cells and require cytoskeletal contractility [14].

As cell migration is a dynamic process involving the continuous remodeling of the cytoskeleton, it follows that substrate stiffness also influences cell morphology and spreading. Several groups have shown that cells generally spread to larger areas on stiffer substrates [12, 14, 15, 16] and that the final spread area also depends on surface ligand availability [16, 17]. There is also data to suggest that stiffer substrates promote cell proliferation, while flexible substrates may induce apoptosis in some cell types [18, 19]. This sensitivity of cell proliferation to substrate stiffness has been linked to H-ras activity (a small GTPase)[18]. Stiffness can also influence stem cell differentiation. In 2006, Engler *et al*. showed mesenchymal stem cell (MSC) lineage selection can be controlled by matrix stiffness and that substrates with mechanical properties mimicking a specific tissue induced MSCs to differentiate into cell types from that tissue [20]. For example, soft substrates mimicking brain matrix were deemed neurogenic, while stiffer substrates mimicking bone were deemed osteogenic.

Recently, Califano and colleagues have shown that substrate stiffness can

influence preference for cell-matrix or cell-cell adhesions in endothelial cells, which can play a large part in tissue self-assembly [16, 21]. Softer substrates were shown to induce preference for cell-cell contacts, initiating the formation of network like structures while stiffer substrates induced preference for cell-matrix contacts, generating monolayers. Along with a preference for cell-matrix contacts was an increase in spread cell area and perimeter. When cell-cell contacts were favored, cells usually exhibited some degree of self-assembly into network-like structures mimicking angiogenesis. These cells in self-assembled networks also had a greater aspect ratio compared to cells on stiffer substrates [16]. These studies highlight the influence of substrate stiffness on tissue self-assembly.

1.2.2 Substrate topography

In vivo, cells encounter topographical cues presented by the ECM. This topography is derived primarily from the structure and organization of ECM proteins, which can vary across tissue types. Cells can also encounter exogenous topography, in the form of biomaterial implants. Depending on the purpose of such implants, knowledge of how cells will react to its surface topography can help guide implant design. In the context of tissue engineering, tight control over biomaterial surface topography is often crucial for the success of an implant. The driving force behind how cells respond to topography is the phenomenon known as contact guidance, where cells will spread or migrate along geometrical cues provided to them. Topography on both the sub-cellular and supra-cellular scale have been shown to influence cell behavior [22].

Just like substrate stiffness, cellular response to surface topography can vary between cell types [22, 23] and is likely dependent on a cell's native environment [11]. Surface topography has a significant influence on cell morphology through its influence on contact guidance. Ridge-groove topographies have been shown to induce cell alignment along the major axis of the pattern as compared to cells on flat substrates [22, 24]. Along with this influence on morphology is an influence on cell migration. Again, cells cultured on ridge-groove patterns will tend to migrate along the pattern [22, 11]. In addition to influencing physical cell parameters, certain topographies have the ability to influence stem cell differentiation [24]. For example, specific disordered nanotopographies have been shown to significantly increase osteospecific differentiation in mesenchymal stem cells [25]. Other topographies on the nanoscale can also modulate the adhesion dynamics mesenchymal stem cells and their gene expression [26, 27, 28].

Common substrates for studying cell response to surface topography are silicon, polydimethylsiloxane (PDMS), and polymethylmethacrylate (PMMA) [29]. Both substrates have surfaces that can be easily modified using photolithography and other fabrication techniques. Using these substrates, topographies with dimensions down to tens of nanometers have been achieved [30, 11, 29].

1.2.3 Expanding the overlap between stiffness and topography

To-date, both substrate stiffness and substrate topography have been studied extensively, however they are not often decoupled from each other. Substrates with controlled topographies tend to have a very high Young's modulus compared to what is found *in vivo* [29, 10]. Conversely, substrates of tunable stiffness

are most often fabricated against flat glass, implying a flat surface. The term topography refers to physical geometric features on the surface of a substrate. This topography can be on the order of nanometers (sub-cellular) up to millimeters (supra-cellular). Here, a method is described for producing substrates where both Young's modulus and surface topography can be independently tuned to examine their combined effects on cellular behavior. Topography on the order of tens of microns is examined in this study. Also described are additional uses of microfabrication techniques in studying cell mechanics as well as relevant design considerations.

CHAPTER 2

PATTERN DESIGN RATIONALE

The first step in any microfabrication process is determining the physical dimensions and characteristics of the desired substrate. For the purpose of these studies, variations on simple geometric shapes were employed. This enabled simple characterization of the end product while providing similarly simple cues for cells to interpret. Micromolding was the primary technique employed here to produce topographical features on a polymer substrate. This process involves casting a polymer in direct contact with a mold to transfer features to the polymer surface. The patterns described here were applied to either micromolding polyacrylamide (PA) for use as cell culture substrates or micromolding polydimethylsiloxane (PDMS) for other molding or stamping applications. All of the features generated here are in silicon (Si). They are recessed (negative) and will produce protruding (positive) features in PA or PDMS.

Figure 2.1 shows the generic XY pattern template used to fabricate the Si molds. X and Y represent feature width and length respectively, while R_X and R_Y indicate the separation radius between features in those directions. All patterns consisted of a simple rectangle or square in the XY-plane that was etched down to specific depths (Z). Feature dimensions ranged from as small as 10 μm to as large as 7 mm (Table 2.1). This XY range was chosen to explore and define the regime of feature sizes that could be effectively transferred to the chosen polymer. Each pattern was etched to several different Z depths to explore pattern fidelity over a range of pattern sizes. Subsets of these patterns were then used to micromold PA or PDMS (for subsequent collagen micromolding), or to

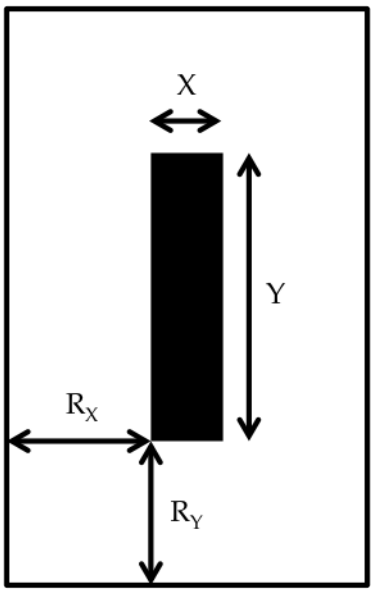

Figure 2.1: X and Y dimensions of patterns introduced to silicon masters. R_X and R_Y represent the radius of separation between features in the respective X and Y directions. Dark regions represent etched area.

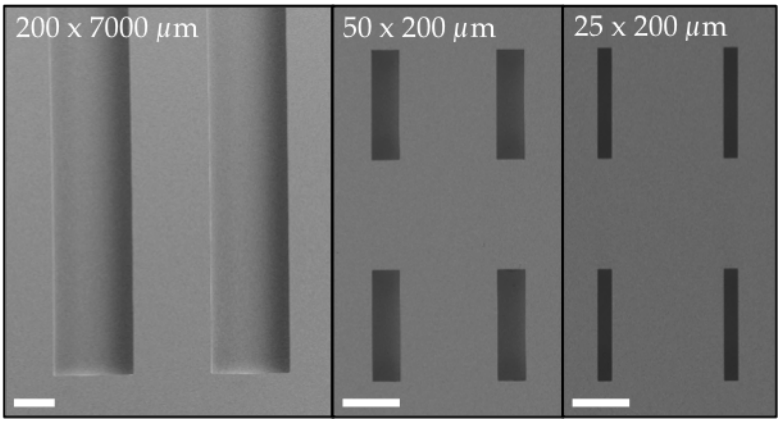

Figure 2.2: Scanning electron micrographs (SEMs) of selected Si masters. Scale bar = 100 μm.

micropattern ligands on PA, as indicated in Table 2.1.

Fabrication involved photolithography to define the XY pattern dimensions (Figure 2.1) followed by deep reactive ion etching (DRIE) to impart depth in

Table 2.1: Si master dimensions. Rightmost column abbreviations indicate micromolding PA, micropatterning PA, and micromolding collagen respectively. Suffix "inv." indicates features are positive rather than negative in the Si master.

Pattern	X (μm)	Y (μm)	Z (μm)	R_X (μm)	R_Y (μm)	μ-mPA	μ-pPA	μ-mCol
10x200	10	200	17	100	100	X	-	-
25x200	25	200	35	100	100	X	-	-
25x200	25	200	80	100	100	X	-	X
50x200	50	200	70	100	100	X	-	X
50x200 inv.	50	200	16	100	100	X	-	-
50x200 inv.	50	200	50	100	100	X	-	-
10x300	10	300	20	250	250	-	X	-
15x300	15	300	21	250	250	-	X	X
15x300	15	300	30	250	250	-	X	X
10x1100	10	1100	20	250	250	-	X	X
10x1100	10	1100	30	250	205	-	X	X
22x22	22	22	20	250	250	X	X	-
22x22	22	22	30	250	250	X	X	-
200x7000	200	7000	20	100	-	X	-	-
200x7000	200	7000	50	100	-	X	-	-
200x7000	200	7000	140	100	-	X	-	-

the Z direction and finally SEM to confirm feature dimensions (Figure 2.2). The specific protocol used to fabricate and characterize these molds can be found in section A.1.1.

CHAPTER 3

MICROMOLDING OF POLYACRYLAMIDE SUBSTRATES OF TUNABLE YOUNG'S MODULUS

3.1 PA as a cell culture substrate of tunable Young's modulus

Historically, polyacrylamide (PA) has been used in electrophoresis to separate molecules of different sizes [31]. More recently, it has become a common substrate for examining cellular response to matrix stiffness [32]. PA is a polymer made up of two primary components: acrylamide (the monomer) and N,N'-methylenebisacrylamide (the crosslinker, commonly called bis-acrylamide). Gel composition is conventionally described by the parameters T and C, where the concentration (w/v) of total acrylamide (acrylamide and bis-acrylamide) is known as T and the percentage of this total that is bis-acrylamide (crosslinker) is known as C. Modulation of these two parameters controls gel properties, including the Young's modulus which can be modulated from tens of pascals up to several hundred kilopascals.

A free-radical polymerization mechanism is employed to generate PA gels from the monomer solution. Two additional components included in the monomer solution are critical to successful and repeatable polymerization.

Tetramethylethylenediamine (TEMED): TEMED is included in the monomer solution at a concentration of 0.046% (v/v) and helps to catalyze free-radical polymerization.

Ammonium persulfate (APS): APS is the last component added to the monomer solution and initiates the free-radical polymerization mechanism, catalyzed by

TEMED. The concentration of APS in the monomer solution at initiation is 0.005% (w/v).

Included in addition to the acrylamide, bis-acrylamide, TEMED and APS are several other components that enable characterization of the gel and its use as a cell culture substrate.

4-(2-hydroxyethyl)-1-piperazineethanesulfonic acid (HEPES): A HEPES buffer solution of 0.25 mM is included in the monomer solution to help maintain physiologic pH.

Fluorescent beads: To visualize the bulk gel, red fluorescent beads (0.5 μm in diameter, carboxylate-modified) are included at 0.01% (w/v). The original bead solution is sonicated for 10 minutes prior to being diluted in water and added to the uninitiated monomer solution.

N-6-((acryloyl)amido)hexanoic acid (N-6): N-6 is included in the gel formulation as a linker molecule that can bind free amine groups [33] such as those present at the N-terminus of a peptide. During gel preparation, N-6 is first dissolved in ethanol before being added to the monomer solution. Any peptide or small molecule having a free amine group can be attached to the gel surface via this linker.

Collagen: Here, rat-tail type-I collagen is linked to the gel surface via the N-6 linker, allowing integrin binding. This makes the gel surface adhesive, as bare PA is non-adhesive to cells [34]. All gels fabricated are incubated with collagen at a concentration of 0.1 mg/mL in 50 mM HEPES.

A summary of the PA gel formulations used and their Young's modulus (as

Table 3.1: Polyacrylamide gel formulations.

E (kPa)	T (%)	C (%)	[Acryl] (%)	[Bis] (%)
1.13	3.40	4.46	3.243	0.151
2.87	5.51	1.96	5.405	0.108
3.55	4.67	4.46	4.459	0.208
2.42	8.16	0.66	8.108	0.054
2.60	8.20	1.15	8.108	0.095
6.14	8.30	2.28	8.108	0.189
11.2	8.49	4.46	8.108	0.378
Untested	8.63	6.02	8.108	0.519
Untested	8.72	7.01	8.108	0.611
11.6	9.63	1.16	9.514	0.111
32.1	13.1	1.15	12.973	0.151
42.5	13.1	2.28	12.973	0.303
>42.5	13.6	4.46	12.973	0.605
Untested	13.8	6.02	12.973	0.830
Untested	13.9	6.98	12.973	0.973

characterized by microball indentation) can be found in Table 3.1.

3.2 Micromolding & Characterization of PA gels

3.2.1 Mechanical testing to measure Young's modulus

A number techniques exist to measure the mechanical properties of PA gels, including tensile testing of gel strips [12], microball indentation [13, 34], micropipette aspiration [35], and rheometry [36]. A microball indentation method was utilized here. In short, a steel microball was placed on the surface of a

flat PA gel containing fluorescent microbeads and the surface deformation was measured using the stage micrometer on a fluorescent microscope. The Young's modulus of the gel was then calculated from the measured deformation using an equation described by Lo and colleagues [13].

$$E = \frac{3(1 - v^2)f}{4d^{3/2}r^{1/2}}$$

Where E is the Young's modulus, v is the Poisson's ratio, f is the force exerted by the microball on the gel, d is the deformation in the gel, and r is the radius of the microball. Deformation measurements were carried out on PA gels submerged in PBS and equilibrated to 37°C. A detailed protocol can be found in section A.1.6. Using this method, gel E values were found to range from approximately 1 kPa to >42 kPa (Table 3.1), a range considerably lower than that reported for polymers such as PDMS [29].

To examine how gel formulation parameters T & C influence E, a linear regression model of our empirical data was constructed (Figure 3.1). A linear model was used here as it is the most straightforward to implement. Relations between polymer composition and mechanical properties such as the Mark-Houwink equation describe mechanical properties as an exponential function of molecular weight. The value of this exponent in such relations however is usually close to 1, making linear models a reasonable alternative. The behavior of E as a function of T and C as revealed by this model agree with other measurements of gel elastic moduli [12, 15, 36]. In general, an increase in either T or C will result in an increase in E. However, from an inspection of the fit, $\frac{\partial E}{\partial T}$ appears to be greater than $\frac{\partial E}{\partial C}$. Important to note here is that T represents the total acrylamide concentration while C only represents the fraction of crosslinker in

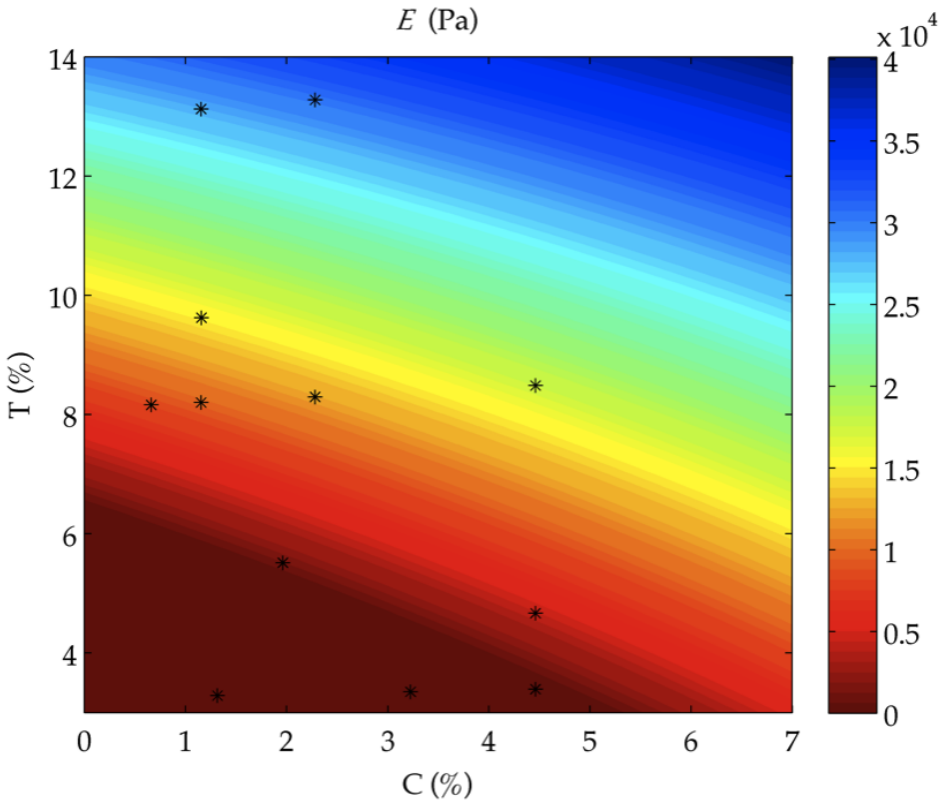

Figure 3.1: Linear fit of E to T vs. C ($R^2 = 0.7837$). Asterisks (*) indicate empirical data points.

that total and is dependent on T itself. A change of 1% in C represents a different physical change depending on T. Therefore it is not surprising that a percentage change in T may carry more weight in changing E than a similar change in C does. These observations agree with previous measurements in the literature [12, 15, 36]. A comparison of how SR_Z and E both vary with T and C confirms that feature SR_Z is not predicted by E. Rather, T and C are better indicators of SR_Z than E is.

An important distinction to make here is the difference between Young's modulus (E, a material property of the gel) and the stiffness of features (a structural property of the features). Based on beam theory, protruding features can

have a different effective stiffness that depends on feature dimensions in addition to the bulk gel Young's modulus [37]. Depending on feature length scale, this phenomenon can affect the substrate stiffness that is perceived by cells.

Variability in measured Young's modulus can be attributed to many sources, similar to those that affect gel structure and swelling. These factors include temperature [36] and TEMED concentration [38]. Additionally, degassing of the monomer solution can affect polymerization rate, much like TEMED does and therefore may affect gel structure and mechanical properties. These factors were kept constant across all gel preparations to control their potential contributions to Young's modulus variability.

3.2.2 Fabrication process flow

Standard PA gel fabrication for cell culture involves gel polymerization between two flat glass coverslips, where one is chemically activated (for gel attachment) and the other is hydrophobic (for gel release). This results in a gel with a flat surface for cell culture. The technique of micromolding was employed here to introduce features onto the gel surface intended for culture (Figure 3.2).

PA gels were fabricated using a protocol modified from Califano *et al*. [16]. First, the Si master mold surface was made hydrophobic by coating it with Rain-X. A droplet of initiated monomer solution (80 μL) was then dispensed onto the surface of the Si master and flattened with a 22x22 μm^2 activated glass coverslip. Polymerization was allowed to occur for 30 minutes and then the activated coverslip was removed with the gel attached. The resulting gel surface was then derivatized with 0.1 mg/mL rat-tail type-I collagen via the N-6 linker.

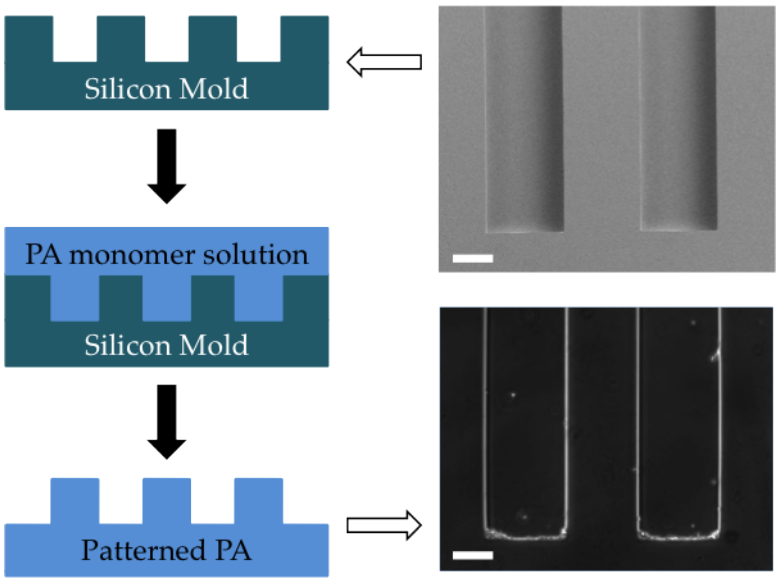

Figure 3.2: Gel fabrication process flow from Si master mold to micro-molded features in PA. Adapted from [1].

Gel substrates were then stored in PBS for up to one week until characterization or culture. A detailed version of this gel fabrication protocol can be found in section A.1.3.

3.2.3 Feature height measurement

To assess the fidelity of the features molded on the PA gel surface, the swelling ratio (SR) parameter was defined as the ratio of a feature dimension (H) to the corresponding mold dimension (H_0).

$$SR = \frac{H}{H_0}$$

When $SR = 1$, the molded feature dimension measured is equal to the master mold dimension. A $SR > 1$ indicates an increase in feature size relative to the

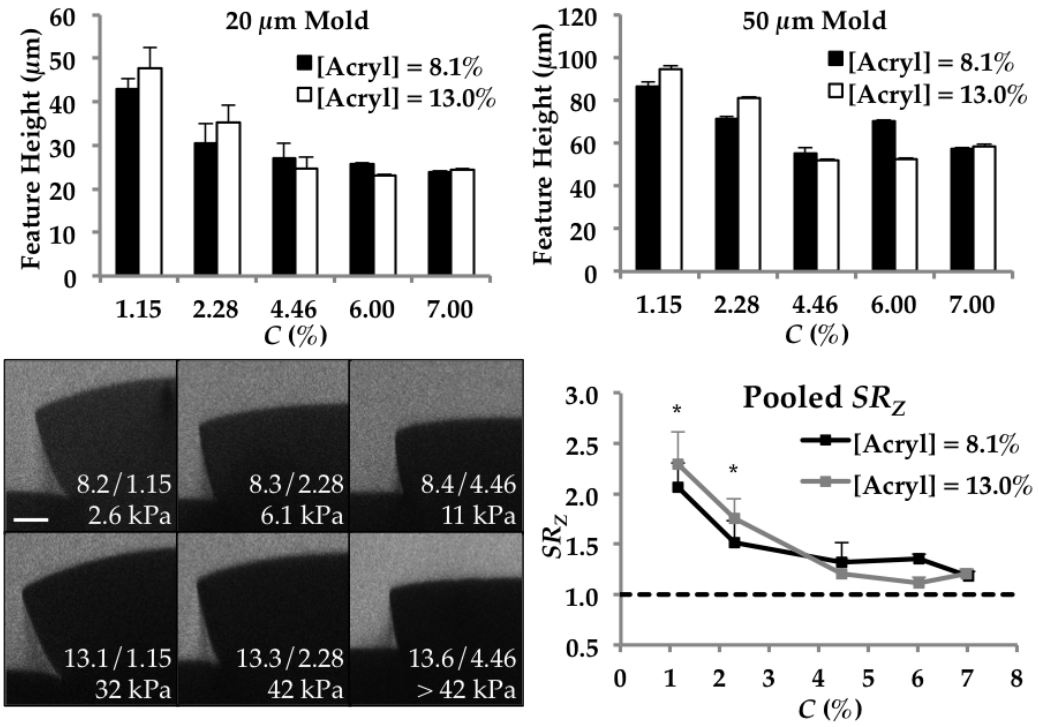

Figure 3.3: Feature swelling as a function of C. 200x7000x20 μm^3 feature heights (top left). 200x7000x50 μm^3 feature heights (top right). Vertical feature cross sections, scale bar = 25 μm (bottom left). Pooled SR_Z for both feature heights, asterisk (*) indicates statistically significant difference from other formulations with $p < 0.05$. Error bars are standard deviation. Adapted from [1].

mold while a $SR < 1$ indicates a decrease in feature size relative to the mold. A swelling ratio can be defined along any feature dimension. Focus is given here to vertical (Z-direction) swelling phenomena, SR_Z, due to its potential impact on perceived substrate stiffness, specifically in the case of sub-cellular topography, which is discussed in-depth later.

To effectively measure the dimensions (and hence SR) of features, micromolded PA gels were immersed into either PBS or complete 199 media containing 40 kDa FITC-conjugated dextran to provide contrast between the gel and solution. Confocal microscopy was used to collect XY and XZ cross-sectional

images of features. Feature dimensions were then extracted from images using NIH ImageJ. A minimum of 10 features per gel were imaged and dimensions were averaged to calculate the SR. A more detailed protocol can be found in section A.1.5.

Previous studies of PA gels [39, 40, 41] indicate that bulk gel swelling varies as a function of both T and C. However, for the range of T explored here ($T < 14\%$), C should be a stronger determinant as evidenced by previous empirical measurements of PA gel swelling by Richards and Temple [39]. The SR_Z values measured from the 200x7000 μm^2 pattern were assessed as a function of C (Figure 3.3). Micromolded features (Figure 3.3) deviate from the master mold in two primary ways:

1. Patterned features have lost some orthogonality.
2. Patterned feature dimensions exceed mold dimensions ($SR > 1$).

These data indicate that deviations from the mold dimensions (SR) and shape are minimized as C is increased. These deviations reach and maintain a minimum at and above $C = 5\%$. This value of C has been previously reported to minimize PA gel pore size [40, 41]. The swelling behavior observed in the vertical (Z-direction) was also observed in the horizontal directions of protruding features cast in swelling-reduced gels with $C \geq 4.5\%$ (Figure 3.4). The 10x200 μm^2 molded features however exhibited a $SR_Z > 1$, which may be due to insufficient wetting of the mold by the monomer solution (Figure 3.4).

Our ultimate goal is to develop methods that create high fidelity patterns that can be reproducibly fabricated. As such, we also investigated variability between gel batches. The standard deviation of feature heights within a gel and

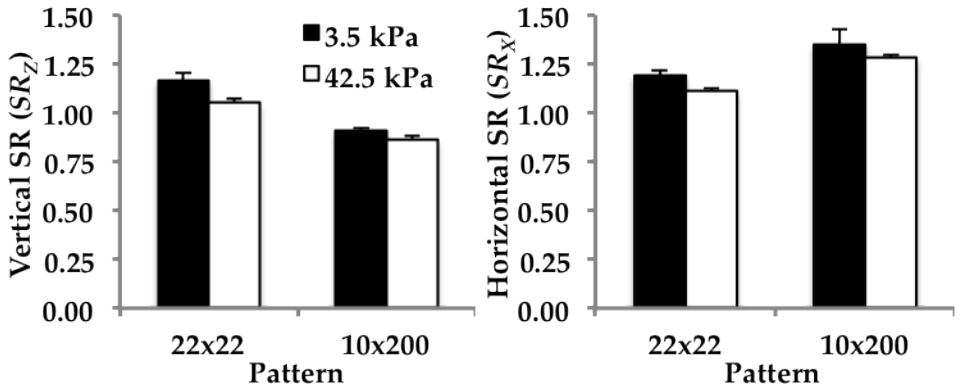

Figure 3.4: Vertical and horizontal SR of small features in gels of reduced swelling ($C \geq 4.5\%$). Error bars are standard deviation.

between multiple gels was compared for a number of formulations (Table 3.2). A population of feature heights measured on the same gel has less variability compared to a population of feature heights measured on different gels. This is likely attributed to human error while manually removing gels from their mold, while preparing the monomer solution, or due to measurement errors such as pipette volume resolution.

3.2.4 Factors influencing pattern fidelity to mold dimensions

Based on the experimental data described above (Figure 3.3), it is clear that the crosslinker content (C) is a primary influence on gel swelling and hence pattern fidelity within the domain of gel formulations explored ($3\% < T < 14\%$ and $0.5\% < C < 7\%$). The measured relationship between gel formulation (T & C) and vertical feature swelling (SR_Z) is modeled in Figure 3.5 for the 200x7000 μm^2 pattern. This relationship presented (Figure 3.5) is based on a linear regression fit of our pooled SR_Z data for 20 μm and 50 μm deep molds. A linear model was chosen based on previous analyses of gel swelling [39]. These results

Table 3.2: Batch variability in protruding feature heights (200x7000x20 μm^3). Adapted from [1].

T/C	E (kPa)	Within a batch	Across pooled batches
8.20/1.15	2.6	±1.652	
8.20/1.15	2.6	±0.893	±2.454
8.20/1.15	2.6	±0.693	
8.30/2.28	6.1	±0.306	
8.30/2.28	6.1	±1.541	±4.592
8.30/2.28	6.1	±1.013	
8.49/4.46	11	±1.055	
8.49/4.46	11	±0.525	±3.448
8.49/4.46	11	±0.504	
13.11/1.15	32	±1.813	
13.11/1.15	32	±1.017	±4.756
13.11/1.15	32	±0.934	
13.28/2.28	42	±5.898	
13.28/2.28	42	±0.500	±4.029
13.28/2.28	42	±0.969	
13.58/4.48	> 42	±0.262	
13.58/4.48	> 42	±0.278	±2.938
13.58/4.48	> 42	±0.282	

correspond with previous measurements and modeling of PA gel swelling as a function of the parameter C [39, 42]. Models from the literature—based on equilibrium swelling theory, originally proposed by Flory and Rehner [43]—indicate that T can also modulate gel swelling, although to a lesser extent than C over the range explored here ($3\% < T < 14\%$).

Based on the regression analysis depicted in Figure 3.5, C needs be kept at or above 5% to produce micromolded gels with minimal feature deviation. Con-

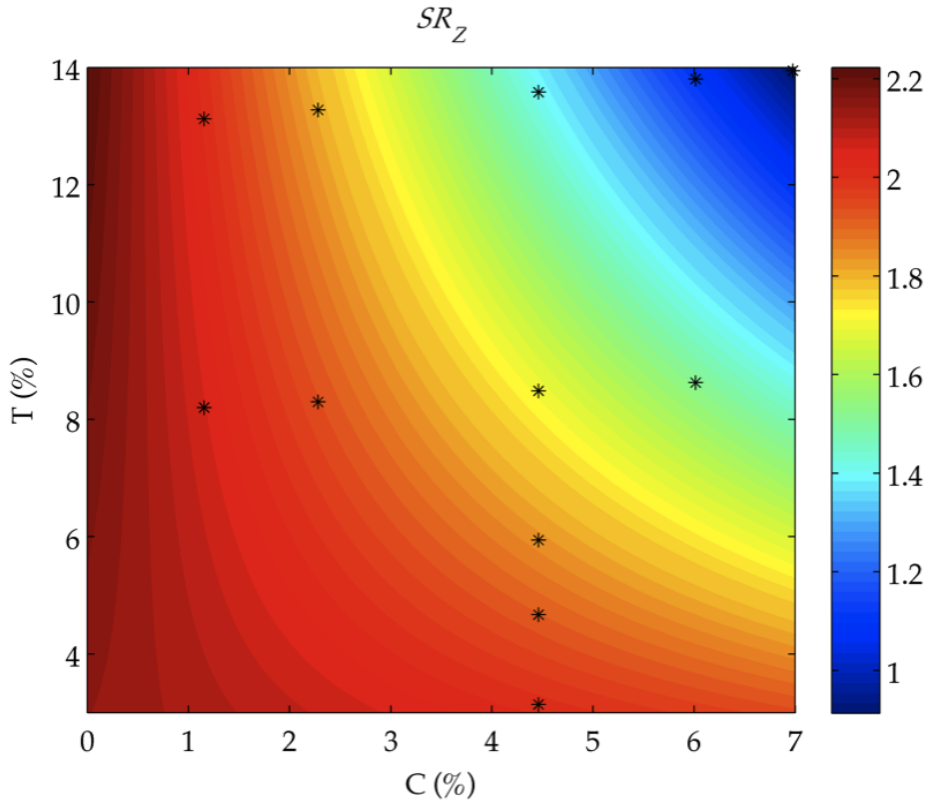

Figure 3.5: Linear fit of SR_Z to T vs. C ($R^2 = 0.3385$). Asterisks (*) indicate empirical data points.

sequently, there is a limit to the range of Young's moduli that may be used to create microfabricated substrates with high pattern fidelity. When a lower modulus is desired and C is at 5%, the T parameter must be decreased in order to maintain favorable pattern fidelity. However, if a greater modulus is desired, either T or C may be increased without loss of pattern fidelity.

Aside from gel formulation, several other factors have been shown to influence the gel structure and swelling properties of PA gels, including ionic solutes [44], temperature [44], pH [44], and TEMED concentration [38]. Although the specific influences of these factors were not studied here, their potential to produce variability was controlled by keeping them constant across all experimen-

tal conditions. Batch variability in feature height (Table 3.2) may be partially attributed to inconsistencies in these factors. Additionally, gel swelling may influence the effective modulus of the gel by changing the mass concentration per unit volume however this was not investigated here.

Comprehensive evaluation of gel swelling as a function of T and C can inform the design of mold patterns that anticipate a certain degree of swelling. This enables the design of molds where gel swelling is harnessed to produce the desired features. The primary drawback to this however, is that molded features do not swell isotropically and lose their orthogonality with respect to the mold. Correcting this would require an examination of swelling as a function of feature geometry.

3.3 Cellular response to micromolded PA features

Contact guidance is a widely observed phenomenon in which cells preferentially spread or move along a geometric cue [45, 46]. Contact guidance due to substrate topography has been extensively characterized [22, 23, 11, 24, 47, 29], however these studies have been primarily on stiff substrates such as PDMS or glass. It is unknown whether the stiffness of the substrate providing contact guidance cues affects the elicited cellular response. The method described above enables these two parameters to be decoupled from one another.

Having characterized the effects of gel formulation on pattern fidelity, a set of formulations were chosen that covered a wide range of E values while maintaining good pattern fidelity ($C \geq 4.46\%$, minimizing SR_Z). Using these formulations, gels with an alternating plateau-trough pattern (the 200x7000 μm^2

pattern) were fabricated, seeded with bovine aortic endothelial cells (BAECs) and the resulting cellular response was characterized. These features presented either a vertical wall or cliff of variable height spaced every 200 μm to the cells. Feature height was molded at either 20 μm (roughly the height of a cell) or 50 μm (taller than a cell). Cell behavior was observed using time-lapse, phase contrast microscopy. Using this system it is possible to examine the combined effects of substrate Young's modulus and substrate topography on cell behavior.

3.3.1 Contact guidance

To examine the qualitative effects of features on cell migration, BAECs were observed on micromolded (200x7000 μm^2) PA gels of varying stiffness (1.1 kPa to > 42 kPa). Cells that physically encountered features exhibited some degree of contact guidance (Figure 3.6) on all patterns and gel formulations tested. The substrates fabricated here present both concave (wall) and convex (cliff) geometric contact guidance cues. The majority of contact guidance observed on the micromolded substrates was in the context of migration, where cells would migrate along the geometric cues rather than remain stationary while in contact. Considering these qualitative observations, cell behavior on micromolded substrates was characterized in terms of two parameters: contact events and contact lengths.

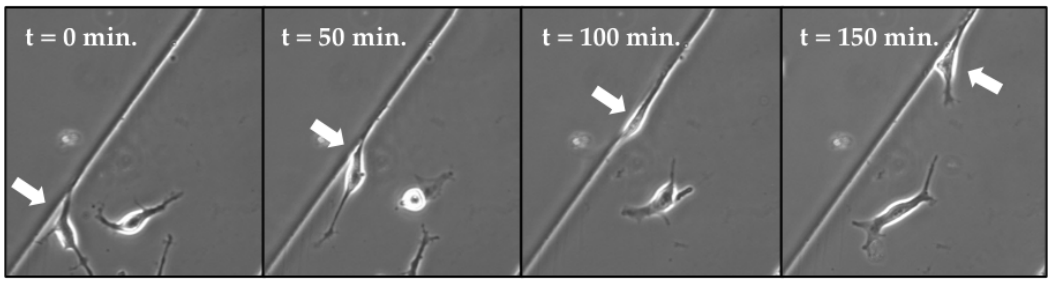

Figure 3.6: Contact guidance can direct BAEC migration. White arrows identify a cell exhibiting contact guidance. Asterisk (*) indicates higher elevation.

3.3.2 Contact events

To determine the simultaneous effects of substrate Young's modulus and feature-induced contact guidance on cell migratory behavior, the outcome of feature contacts was quantified as a proportion of the total cell population observed per field of view. Cells were seeded on micromolded PA gels and observed with phase contrast microscopy for a period of 12 hours starting 4 hours post-seeding. Each completely observable incidence of a cell contacting a feature was termed a contact event. These contact events were then categorized into one of three groups based on the time spent in contact with the feature and the change in cell location relative to the feature:

- Δ State = cell contacts feature, climbs up/down, departs in $<$2 hours
- Remain = cell contacts feature, remains in contact for $>$2 hours
- Depart = cell contacts feature, departs on same side in $<$2 hours

Of the events that were observed, cells remain in contact with the wall for 2 hours on average. This time was used as a threshold for categorizing contact events (Figure 3.7).

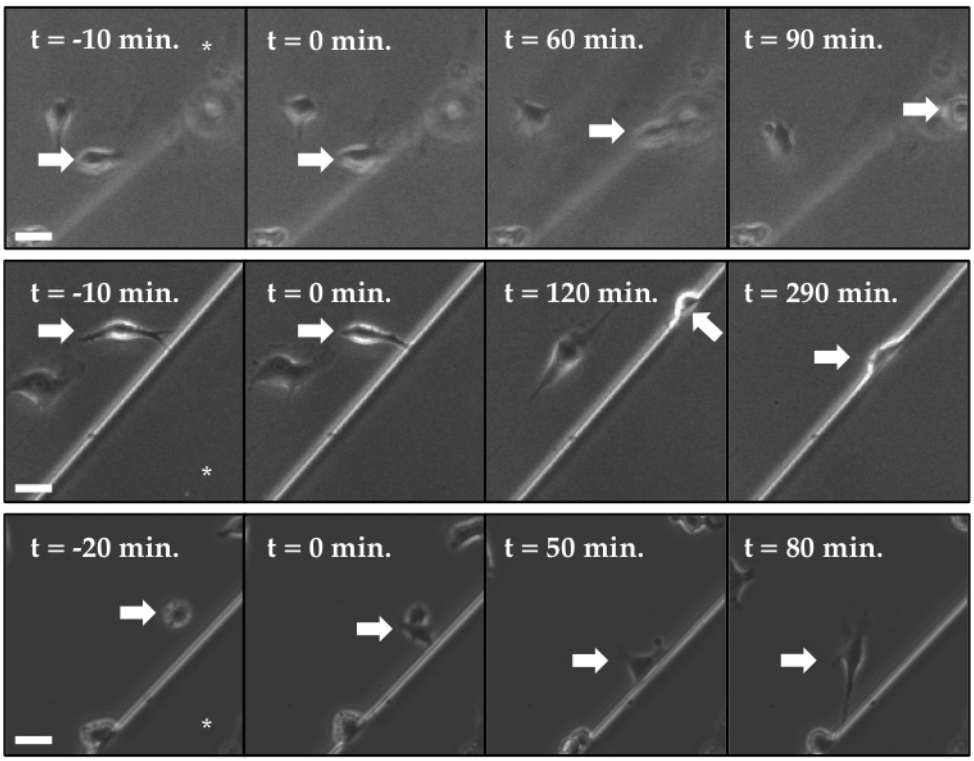

Figure 3.7: Contact event examples. Δ State (top row). Remain (middle row). Depart (bottom row). White arrows indicate cells exhibiting the described contact event. Scale bar = 30 μm. Asterisk (*) indicates higher elevation.

Contact events were quantified as a function of substrate Young's modulus and feature height (Figure 3.8). The results reveal no significant difference in contact event distribution with substrate Young's modulus or feature height. A recent study suggests that left superclavicular lymph node cells (LNCaP) and highly metastatic prostate cancer cells (PC-3) have the ability to climb tall, square (100x100μm^2) features [48], however this behavior is not observed here. The absence of vertical contact guidance cues may explain why cells do not climb or down features but rather prefer in some capacity to remain in contact with features. Our data indicate that a change in substrate Young's modulus does not change the apparent influence of convex and concave (wall and cliff)

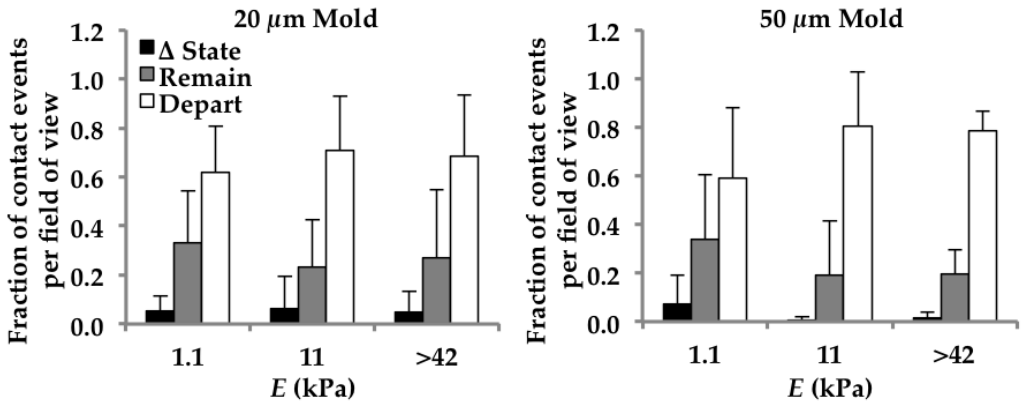

Figure 3.8: Contact event distributions vs. E. Error bars are standard deviation. Adapted from [1].

linear geometric cues on directing the outcome of contact events as defined here.

3.3.3 Contact lengths

To quantify degree of contact guidance, the average cell spread length parallel to a feature wall or cliff was measured manually with NIH ImageJ at 8 hours post-seeding to allow cells to fully spread (Figure 3.9). This metric can be interpreted as the affinity of a cell towards a contact guidance cue.

Cells exhibited significantly longer contact lengths with increasing substrate Young's modulus (Figure 3.9, right). This result suggests cells prefer more contact with features of greater moduli and correlates well with previous studies showing that cells reach a larger spread area on substrates with higher Young's modulus [16]. It also suggests that cellular sensitivity to contact guidance cues may be reduced when the cues are more mechanically compliant. Conversely, cellular sensitivity to contact guidance cues may be increased when cells favor cell-matrix interactions, as is the case on stiffer substrates [16].

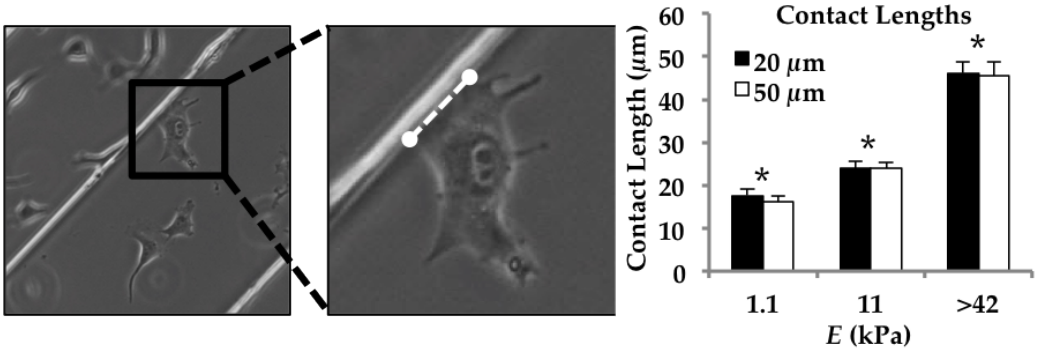

Figure 3.9: Contact length definition (left), dotted line is approximately 33 μm. Contact lengths as a function of E (right), adopted from [1]. Asterisk (*) indicates statistically significant difference between E values ($p < 0.05$). Error bars are standard error of the mean.

CHAPTER 4

MICROPATTERNING OF ADHESIVE LIGANDS ON FLAT PA GELS: THE ROLE OF SWELLING

Investigating the effects of PA gel swelling on micromolded features in PA gels revealed the influence of gel formulation on patterned feature fidelity. This naturally raised the question of whether gel swelling affects the efficiency of other microfabrication techniques used with PA gels, namely the micropatterning of adhesive ligands to a flat gel surface. This method is commonly used for constraining the shape of single or multiple cells on a gel surface by controlling surface adhesivity. Once patterned, the effects of cell shape on other factors such as cytoskeletal structure, cell contractility, cellular protrusions [49, 50, 51], can then be examined as a function of stiffness. Here, the influence of gel formulation on the spacing fidelity of micropatterned ligands is examined.

To pattern the surface of gels, a method adopted from Rape *et al*. [51] was used. In short, this method involves microcontact-printing islands of collagen onto the non-activated top glass coverslip prior to use of the coverslip in the gel polymerization setup. The printed islands of collagen are then transferred to the gel surface during polymerization, yielding adhesive and non-adhesive regions. Adhesive islands (25x200 μm^2) of rat-tail type-I collagen were patterned onto the surface of flat PA gels of the same stiffness but with different theorized degrees of gel swelling. Both gel formulations had a measured Young's modulus of approximately 11 kPa, but different composition (T/C = 8.49/4.46 or T/C = 9.63/1.16). These T/C pairings were chosen based on the above analysis to exhibit appreciably different degrees of swelling. For each formulation, the spacing of micropatterned ligand was quantified as a function of initial

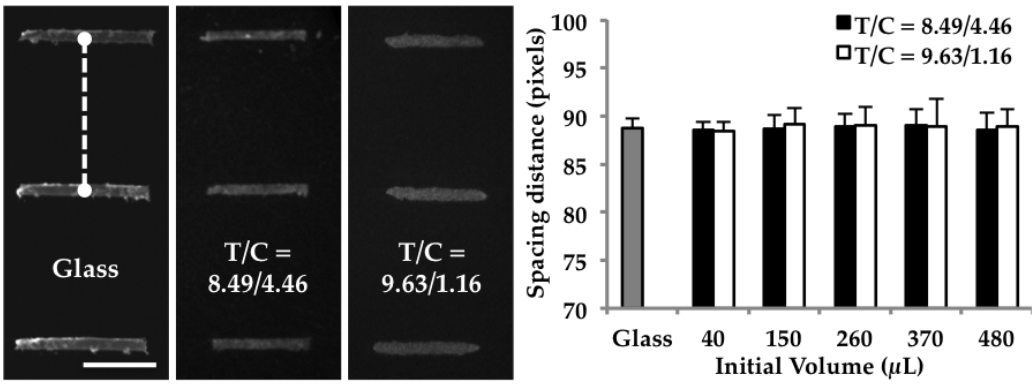

Figure 4.1: Ligand spacing by formulation and volume. Representative images of surface patterned ligands, the dotted line indicates the distance quantified, scale bar = 100 μm (right). Quantification of this distance is displayed as a function of gel initial volume (left). Error bars are standard deviation. Adapted from [1].

monomer volume. Increasing the initial monomer volume increases the distance from which the patterned surface is from the constrained bottom of the gel, potentially exaggerating any swelling effects that may be present. Adhesive islands of collagen were visualized through fluorescent immunostaining and pattern spacing was assessed using NIH ImageJ.

The average pattern spacing on all gel surfaces examined is not statistically different from the spacing on a non-swelling (glass) control surface (Figure 4.1), thus indicating that gel formulation is not affecting the spacing fidelity of surface-patterned ligands.

To confirm that the gels are indeed swelling to different degrees, bulk gel heights were measured using the same formulations and initial volumes (Figure 4.2). For all initial volumes except 40 μL, the swelling formulation (T/C = 9.63/1.16) is significantly taller than the non-swelling formulation (T/C = 8.49/4.46) and the expected gel height.

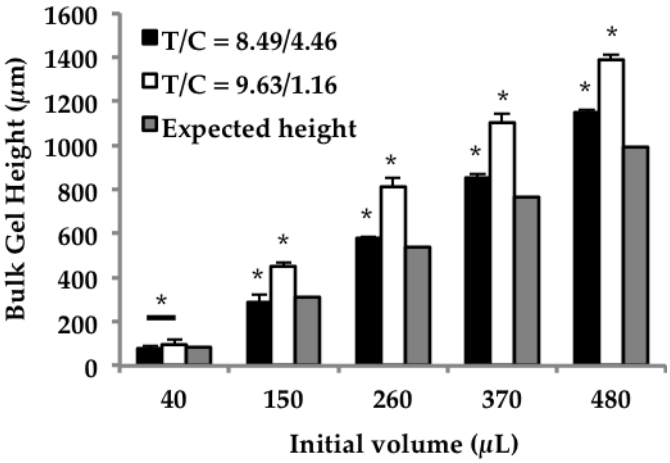

Figure 4.2: Bulk gel height vs. initial volume. Asterisk (*) indicates statistically significant difference from other experimental groups ($p < 0.05$). Error bars are standard deviation. Adapted from [1].

Here it is shown that gel formulation does not appreciably influence the spacing of surface-patterned ligands. This is in stark contrast to the significant role that gel formulation plays in determining the fidelity of micromolded surface features. One possible explanation is that because the gel is flat, there is no horizontal void for it to fill via swelling, thus no deviation in pattern spacing is observed. Feature swelling is observed with protruding features because there is a horizontal void to fill through swelling. A second explanation is that the swelling detection method—essentially a measure of plane strain—does not have sufficient resolution to detect the small amount of swelling that may be occurring. In either case, it is clear that gel formulation is not a significant factor in determining the fidelity of surface-patterned ligands on the length scale investigated here.

CHAPTER 5

CONCLUSION & OUTLOOK

5.1 Future directions: Micromolding PA

The importance of micro- and nano-fabrication techniques in studying cell and tissue behavior continues to grow as researchers realize the immense influence the microenvironment has on proper biological function [22, 23, 8, 29, 24, 10, 21, 3]. Assessed here is the application of two common microfabrication techniques to PA hydrogels. This research provides a method for investigating two factors influential in determining cell behavior that are not often decoupled from one another. Ideally, this method will serve as a platform for insightful future studies. Listed here are only a few current and potential future applications of micromolding PA gel substrates to study cell behavior.

5.1.1 Sub-cellular vs. Supra-cellular topography

The cellular studies described above dealt with topographical features with sizes equal to and greater than that of a cell. Current literature on topographical control of cells indicates that features on the sub-cellular scale also significantly influence cell behavior [22, 23, 11, 24, 47, 29]. As such, future studies with micromolded PA should incorporate topography on such length scales. This would allow for a direct examination of how the stiffness of features influences the elicited cellular response. When working with protruding features on this length scale, a distinction must be made between the modulus of the material and the perceived stiffness of the surface. Cells located on the top of an array of

sub-cellular scale features will perceive a substrate stiffness that is essentially a function of feature dimensions [37, 52, 53].

5.2 Multicellular and tissue-scale studies

Additionally, single-cell behavior was given focus in this study. Substrate Young's modulus has been shown to strongly influence the self-assembly of endothelial cell network structures [16] and tissue behaviors in other cell types [54]. Given that topography can bias single-cell shape and migration [22, 23, 11, 47], it is likely that the introduction of subcellular topography to compliant substrates can bias the morphology of endothelial cell networks and other tissue structures.

5.3 Future directions: Micromolding collagen

5.3.1 Rationale and Method

While PA substrates are incredibly useful for studying cell mechanics in two dimensions, PA is synthetic with a structure cells do not actively remodel. For probing the influence of mechanics on cell behavior in three dimensions, collagen hydrogels afford a more attractive set of advantages. Collagen is a ubiquitous structural ECM protein, can be bound by integrins, and can be remodeled or modified by most cell types. The mechanical properties of collagen can be tuned in two ways. Increasing the concentration of collagen will increase the stiffness of the gel, however this also increases the availability of integrin

binding sites. Alternatively, collagen glycation [55, 56] increases gel stiffness through crosslinking and avoids increasing integrin ligand density, decoupling the two parameters. These qualities make hydrogels of collagen ideal for studying angiogenesis and cell invasion, processes where cellular manipulation of the surrounding matrix and its mechanics is a key event [6, 5].

Further control over the microenvironment collagen hydrogel substrates provide can be achieved by micromolding. Traditionally, cells are simply embedded in collagen by mixing a cell suspension into the neutralized collagen solution prior to polymerization. A soft-lithography method recently developed by Nelson *et al*. [2, 57] enables the production of defined three-dimensional microenvironments into which cells can be seeded. Briefly, neutralized collagen is polymerized while in contact with a PDMS stamp containing positive features. Once the collagen has polymerized, the stamp is removed leaving the negative of its pattern imprinted on the collagen surface. This pattern is identical to what is on the Si master used to create the stamp. The surface-patterned collagen is then seeded with a cell suspension and finally covered with a flat slab of collagen, creating a three-dimensional environment in which to observe cellular activity (Figure 5.1). This method can be applied to study endothelial self-assembly and cancer cell metastasis in three dimensions as a function of matrix stiffness.

5.3.2 Endothelial cell self-assembly in three dimensions

Recently, many similarities between the signaling pathways controlling angiogenesis and epithelial tissue assembly have been revealed [5]. This begs the

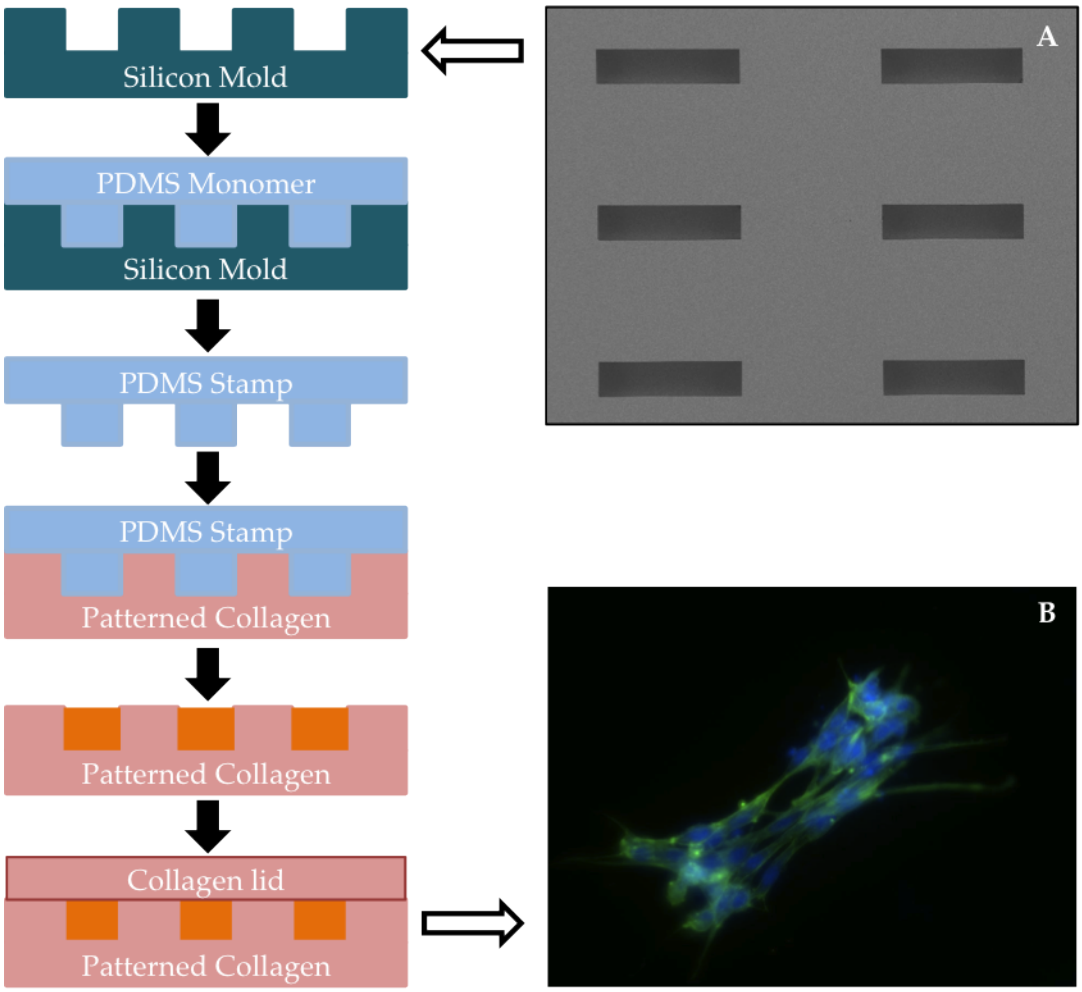

Figure 5.1: Collagen micromolding process flow, from a Si mold (A) to a seeded collagen channel (B). Adapted from [2].

question of whether mechanical cues also bear similar influences on the assembly of both tissue types. The self-assembly and morphogenesis of epithelial tissue structures in collagen has been studied extensively by Nelson and colleagues [57, 2, 58, 59, 60, 61]. Their results suggest that stiffer matrices can induce branching of patterned tubules and that areas of high endogenous matrix stress also induce branching [60]. Taking an analogous approach by seeding endothelial cells into similarly sized tubules while modulating matrix stiffness would reveal if behaviors observed in epithelial cells translates to endothelial

Figure 5.2: Quantification of cell location in micromolded collagen channels [2]. Example images are taken from endothelial cells cultured for 48 hours in 50x200 μm micromolded channels in 6.0 mg/mL collagen. Gray-scale images of nuclei (left) are converted to binary (middle) before being stacked for calculating the frequency of cell location (right), warmer colors indicate higher frequency. Scale bar = 50 μm.

cells. Several Si master molds have been fabricated at a variety of different dimensions (Table 2.1) that are suitable for fabricate PDMS stamps to micromold collagen wells of an appropriate size.

Potential experiments would involve seeding endothelial cells within rectangular wells in collagen and modulating matrix stiffness through gel glycation. Calculating cell location frequency [57, 2] over multiple patterned wells would reveal the degree of branching from the tubules (Figure 5.2) as a function of matrix stiffness and culture time. The effects of soluble factors on branching behaviors in the presence of mechanical cues could also be explored through addition of exogenous growth factors. Preliminary work has validated the feasibility of this method for observing endothelial cell behavior (Figure 5.2).

5.4 Limitations & drawbacks of micromolding PA

As with any tool for studying biology, micromolding of PA has limitations that need to be considered when designing experiments. Many of the limitations described here for micromolded PA gels are also pertinent to the micromolding of collagen and other polymers.

5.4.1 Lower limit of pattern fidelity at low T values

Apparent from the swelling behavior of PA, gels with low T values (and hence low E values, < 1 kPa) will inevitably exhibit a substantial degree of swelling. This may hinder efficient pattern transfer, as features in soft gels are more susceptible to plastic shear deformations that can occur while removing the polymerized gel from its mold. From this, it is likely that a lower threshold of gel stiffness exists at which features will not properly transfer to the gel surface. This threshold most likely lies below 1 kPa, as attempts to micromold softer gels did not consistently produce acceptable features. Additionally, features with a large aspect ratio may deform under their own weight if the gel is too soft.

5.4.2 Lower limit to topography dimensions

Analogously, there are also limits on the minimum topographical dimensions that can be transferred to a PA gel surface. PA has a pore size calculated on the order of tens of nanometers to a couple hundred nm [40, 41, 42], which itself places a limit on the smallest topographical dimension that can be effectively

patterned onto the gel surface. The conformations of any surface-linked proteins will also contribute in raising the minimum size dimension that can be effectively patterned. Therefore, studying very shallow topography known to affect cell behavior [22, 23] may not be possible with this system.

5.4.3 Polymer structure at the gel-mold interface

One gel property not investigated here is the mesh structure of micromolded PA. Transmission electron studies of PA gels have shown that the gel surface structure may differ significantly from the bulk structure [40]. It is possible that the introduction of topography influences the polymerization kinetics near the gel surface and hence the resulting gel properties. However, the presented feature swelling data closely mimics observed bulk gel swelling behavior in the literature [39, 42], suggesting that micromolding likely has minimal effects on bulk gel properties. It is possible however, that smaller features may be more affected by changes in gel structure at the gel-mold interface.

5.4.4 Gel release requires a hydrophobic mold surface

Gel release from the mold is likely the greatest source of feature size variability because it can subject the molded features to shear deformation. In the ideal case, gels are released from the Si master mold by evenly lifting the activated glass in the vertical direction. Such release without imparting shear stress to the molded features is quite difficult to achieve manually. Increasing mold hydrophobicity can minimize deformation of features during release. In the pro-

tocol described here, Rain-X is used to prevent adhesion of the polymerized gel to the mold surface. However, the introduction of too much hydrophobicity may prevent the monomer solution from completely wetting the mold surface thereby hindering pattern transfer, especially for smaller features. Insufficient mold wetting by the monomer solution may explain why features created with the smallest mold dimensions (10x200 μm^2) exhibit a $SR_Z < 1$ (Figure 3.4).

5.4.5 Local stiffness of features vs. bulk gel stiffness

A distinction should be made between the Young's modulus of the bulk gel and the effective stiffness of the patterned features. Presented here are substrates whose bulk Young's modulus can be tuned. The effective stiffness of the molded topography will depend on both feature geometry and the bulk Young's modulus. This distinction is particularly important when creating topography that is smaller than the scale of a cell. Further discussion on effective feature stiffness as well as an example system utilizing feature geometry to modulate effective stiffness has been explored by the Chen group [37].

APPENDIX A

APPENDIX

A.1 Materials & Methods

A.1.1 Silicon master fabrication

Computer aided design of mask layouts was carried out using L-Edit software (Tanner EDA). Once completed, mask layouts were transferred to a PG 3600F Mask Writer and written onto 7-inch chrome mask blanks. Completed masks were stored under cleanroom conditions until use in photolithography. 100 mm diameter N-type silicon wafers were first primed with P-20 primer prior to being spin coated with a 2-3 μm layer of Megaposit™SPR™-220-3.0 photoresist (Rohm and Haas Company, Philadelphia, PA). Spin coated wafers were pre-baked for 90 seconds at 115°C before being exposed on a GCA 6300 DSW projection mask aligner, 5X g-line stepper, using the completed masks. Exposed wafers were then post-baked for 90 seconds at 115°C before being developed using an MIF developer. Exposed and developed wafers were etched using a Bosch etch process on either a Unaxis 770 Deep Si Etcher or an Oerlikon Versaline Deep Si Etcher. Remaining resist was stripped prior to confirming feature dimensions with scanning electron microscopy. Etched features were visualized using a Zeiss Ultra 55 scanning electron microscope. Surface feature dimensions in the xy-plane were confirmed through visual inspection. Feature depths were calculated by imaging samples at a tilt angle and back calculating feature depth. All silicon microfabrication was carried out at the Cornell Nanoscale Facility (CNF).

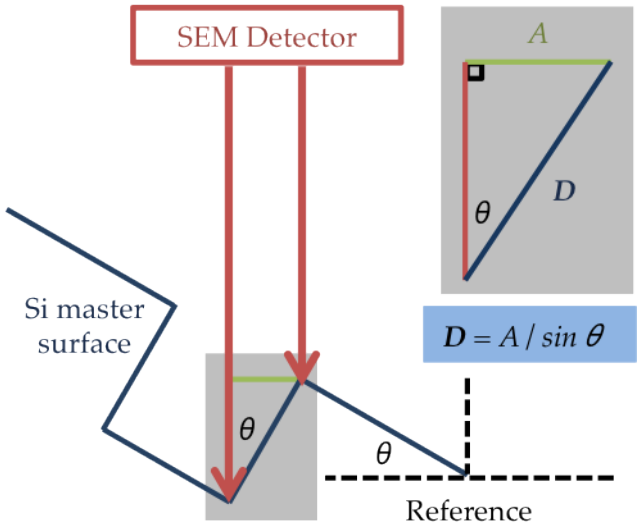

Figure A.1: Feature depth calculation. The observed feature height (A) is divided by the sine of the tilt angle (θ) to obtain the actual feature depth (D).

Figure A.1 illustrates the sample orientation, variables, and equation used in calculating feature depth. Multiple measurements were made across a single wafer and the resulting depths were averaged to obtain an acceptable feature depth.

A.1.2 PDMS casting

Select Si masters were used to fabricate PDMS stamps for either surface patterning ligands on PA or micromolding collagen. Wafer surfaces were first cleaned using acetone and then ethanol before being dried with a pressurized stream of air. Wafers were spin coated with Sigmacote (Sigma-Aldrich, St. Louis, MO) to ensure PDMS release before being placed in the bottom of a 140 mm diameter petri dish. PDMS was prepared in a 10:1 monomer to initiator ratio and degassed under a vacuum pump at least three times before being poured into the

dish. The PDMS was allowed to cure for 2 hours at 60°C. Cured PDMS was then cooled to room temperature before being cut into stamps of desired dimensions. PDMS casting was carried out at Cornell's Nanobiotechnology Center (NBTC) facilities.

A.1.3 Generic PA gel fabrication

To enable gel attachment to coverslips for ease of handling, glass coverslips were activated using a method described by Califano *et al*.[16]. One side of 22 x 22 mm^2 glass coverslips (No. 2, VWR, West Chester, PA) were first heated over a Bunsen burner flame before being coated with 0.1 N sodium hydroxide (Sigma-Aldrich, St. Louis, MO) and allowed to dry in a fume hood. The coverslip surfaces were incubated with 3-aminopropyl-trimethoxysilane (Sigma-Aldrich, St. Louis, MO) for 10 minutes and then washed in 18.2 MΩ cm purified deionized water. Finally the coverslip surfaces were incubated with a 0.5% solution of glutaraldehyde (Sigma-Aldrich, St. Louis, MO) in phosphate buffered saline (Invitrogen, Carlsbad, CA) and washed again in 18.2 MΩ cm purified deionized water.

Polyacrylamide monomer solutions were prepared with the component concentrations listed in Table 3.1 using 40% (w/v) stock acrylamide solution and 2% (w/v) stock N,N'-methylene-bis-acrylamide stock solution (Bio-Rad, Hercules, CA) in 4-(2-hydroxyethyl)-1-piperazineethanesulfonic acid (HEPES, pH 6.0, Sigma-Aldrich, St. Louis, MO) with 0.05% N,N,N,N-tetramethylethylenediamine (Bio-Rad, Hercules, CA). For linking collagen to the gel surface, 20 μmol/mL of N-6 ((acryloyl)amido)hexanoic acid (N-6 linker,

synthesized according to the methods of Pless *et al*. [33]) was included. Gel solutions intended for mechanical testing or for feature visualization were prepared with 0.01% 0.5 μm carboxylate modified fluorescent beads (Molecular Probes, Carlsbad, CA). Prepared solutions were degassed for 30 minutes under a vacuum to remove dissolved oxygen.

All gel polymerization was carried out between the activated glass coverslip and a second glass surface. The properties of the second glass surface were chosen depending on the final use of the gel. For a flat gel, the second surface was an 18 mm diameter glass coverslip (No. 2, VWR, West Chester, PA) coated with Rain-X to facilitate release of the polymerized gel. For a micromolded gel, the second surface was a silicon master mold (containing surface feature dimensions listed in Table 2.1) coated with Rain-X to facilitate release of the polymerized gel. For a micropatterned gel, the second surface was a micropatterned glass coverslip prepared as described by Rape *et al*. [51]. Briefly, polydimethylsiloxane (PDMS) stamps (fabricated from the custom Si molds listed in Table 2.1) were inked for 30 min with 0.1 mg/mL type-I rat-tail collagen (BD, Franklin Lakes, NJ) that had been reacted on ice for 2 hours with 50 mM HEPES containing 20 μmol/mL N-6 linker dissolved in ethanol. 22 x 22 mm^2 glass coverslips were stamped with the inked PDMS surfaces for 5 minutes at room temperature prior to being used as the top surface for gel polymerization. Prepared monomer solutions were initiated by the addition of ammonium persulfate (Bio-Rad, Hercules, CA) at a concentration of 0.005% (w/v). For all gels, polymerization was carried out for 30 minutes between two parallel glass surfaces as described above. Polymerized gels attached to activated glass coverslips were manually removed from their respective molds and incubated for 2 hours at 4°C with 0.1 mg/mL type-I rat-tail collagen in 50 mM HEPES. Mi-

cropatterned gels were not subjected to this step in order to preserve the ligand patterning on their surface. Finally all gels were incubated for 30 minutes with 0.1% ethanolamine (Sigma) in pH 8.0 HEPES before being placed in PBS and stored at 4°C until use.

A.1.4 Cell culture

Bovine aortic endothelial cells of passage 11-12 were maintained at 37°C and 5% CO_2 in Medium 199 (Invitrogen, Carlsbad, CA) containing 10% FetalClone III (HyClone, Logan, UT), 1% penicillin/streptomycin, 1% minimum essential medium (MEM) vitamins (Mediatech, Manassas, VA), and 1% MEM amino acids (Invitrogen).

A.1.5 Imaging

Confocal microscopy for SR measurements

Micromolded PA gels were immersed in either Medium 199 or PBS containing 17.5 mM 40-kDa fluorescein isothiocyanate (FITC)-conjugated dextran (Sigma) and imaged using a Leica SP2 confocal microscope to obtain XY and XZ cross sectional images. A minimum of 10 features per gel were analyzed using NIH ImageJ to determine feature dimensions.

Time-lapse phase-contrast microscopy

Micromolded PA gels were placed in the bottom of 6-well plates and seeded with 15,000 cells/well. Cells were allowed to spread for a minimum of 5 hours before being subjected to time-lapse phase contrast microscopy (at 37°C, 5% CO_2) on a Zeiss Z1 inverted microscope. Images were collected every 10 minutes for at least 12 hours. Cell behavior was analyzed from the collected images using NIH ImageJ.

Fixing and staining of cells in micromolded collagen

Samples were blocked with 0.02% (v/v) Tween 20 (JT Baker, Phillipsburg, NJ) in PBS with 3% (w/v) bovine serum albumin (BSA, Sigma). Gels were incubated 1:50 with rabbit anti-rat collagen antibody (Santa Cruz Biotechnology, Santa Cruz, CA) in PBS/1% (w/v) BSA and a 1:200 FITC-conjugated goat anti-rabbit antibody (Santa Cruz). Patterned collagen was imaged with a Zeiss confocal microscope with a Hamamatsu ORCA-ER camera. Images of micropatterned PA gels were analyzed by measuring the perpendicular distance between the long axes of adjacent patterned features with NIH ImageJ.

Staining of micropatterned ligands

Cells were fixed by incubating samples for 30 minutes with 3.7% formaldehyde in PBS. Samples were washed three times with PBS, permeabilized with 1% (v/v) Triton in PBS and blocked with 3% (w/v) BSA (Sigma) in PBS/0.02% (v/v) Tween 20. F-actin was labeled by incubating samples with AlexaFluor 488 Phalloidin (Molecular Probes) in PBS for 2 hours followed by three more

washes in PBS. Nuclei were then labeled by incubating with 4',6-diamidino-2-phenylindole (DAPI, Sigma) 1:10 in 18.2 MΩ cm purified deionized water for 10 minutes, followed by three more washes in PBS. Stained samples were imaged on a Zeiss Z1 inverted microscope.

A.1.6 Mechanical testing of PA gels

Flat PA gels were fabricated using 80 μL of monomer solution containing 0.01% (w/v) fluorescent beads for mechanical testing. Gels were submerged in PBS at 37°C on a Zeiss Z1 inverted microscope and allowed to equilibrate before indentation measurements were made. Using forceps, a steel microball (0.64 mm in diameter) was placed on the surface of the gel. The microscope was then focused on the interface of the microball with the gel surface and the stage micrometer position was recorded. Using a magnet, the steel microball was removed from the gel surface and the top of the gel was then focused on to obtain a second stage micrometer position. The difference in stage Z-position was then calculated as the indentation depth of the microball d, and used to calculate the Young's modulus of the gel with the following equation described by Lo and colleagues [13]:

$$E = \frac{3(1-v^2)f}{4d^{3/2}r^{1/2}}$$

Where E is the Young's modulus, v is the Poisson's ratio of the gel (assumed to be 0.3), f is the force of the microball on the gel corrected for buoyancy, and r is the radius of the microball. At least five deformation measurements per gel were made on at least two gels to determine the Young's modulus of a given gel

formulation. Using this method and steel microball size, the maximum Young's modulus (smallest deformation) measured was 42 kPa. Gels for which no deformation could be measured were assumed to have a Young's modulus >42 kPa.

A.1.7 Micromolding of features in collagen

Collagen micromolding was performed using the protocol published by Nelson and colleagues [2]. Preliminary cell location analysis was performed using a custom MATLAB script.

A.1.8 Statistical Analysis

Linear regression statistics were obtained with the regress function in MATLAB 2009b (The MathWorks, Natick, MA). Single- or multi-way analysis of variance was performed on the collected data using JMP 8.0 (SAS Institute Inc., Cary, NC) to determine statistical significance with $p < 0.05$.

A.1.9 Data analysis

Described here are various MATLAB scripts developed for data analysis applications including linear regression (Figure 3.5 and Figure 3.1) and image processing (Figure 5.2).

Code used to perform linear regression of E with T and C from empirical data (Figure 3.1)

```
% Table of C, T, and E values
CTE = [ 1.316,3.286,307.491;
        3.226,3.351,1227.928;
        4.459,3.395,1128.307;
        4.459,4.668,3546.642;
        1.961,5.514,2866.673;
        0.662,8.162,2423.400;
        1.153,8.203,2599.969;
        2.280,8.297,6140.423;
        4.459,8.486,11179.817;
        1.157,9.625,11515.014;
        1.153,13.124,32098.833;
        2.280,13.276,42484.234;];

% Extract T, C, and E variables
C = CTE(:,1);
T = CTE(:,2);
E = CTE(:,3);

% Set up regression
X = [ones(size(C)) C T C.*T];
[b,bint,re,rint,Estats] = regress(E,X);

% Set axis ranges & regression
Cfit = 0:0.1:7;
Tfit = 3:0.1:14;
[CFIT,TFIT] = meshgrid(Cfit,Tfit);
EFIT = b(1) + b(2)*CFIT + b(3)*TFIT + b(4)*CFIT.*TFIT;

% Contour plot
v = min(min(EFIT)):500:max(max(EFIT));
figure, [c,h] = contourf(CFIT,TFIT,EFIT,v);
title('\itE  \rm(Pa)'),xlabel('C (%)'), ylabel('T (%)')
set(h,'EdgeColor','none');
colormap(flipud(colormap));
caxis([0 max(max(EFIT))]);
colorbar;

% Overlay location of empirical TC data points
hold on
scatter(C,T,'*k')
```

Code used to perform linear regression of SR_Z with T and C from empirical data (Figure 3.5)

```
% Table of T, C, and SR values
CTSR = [1.153,8.203,2.071;
        1.153,13.124,2.293;
        2.280,8.297,1.521;
        2.280,13.276,1.755;
        4.459,3.140,1.907;
        4.459,4.670,1.440;
        4.459,5.941,3.365;
        4.459,8.486,1.316;
        4.459,13.578,1.206;
        6.015,8.627,1.355;
        6.015,13.803,1.110;
        7.006,8.720,1.183;
        6.977,13.946,1.207;];

% Extract T, C, and SR variables
C = CTSR(:,1);
T = CTSR(:,2);
SR = CTSR(:,3);

% Set up regression
X = [ones(size(C)) C T C.*T];
[b,bint,r,rint,SRstats] = regress(SR,X);

% Set axis ranges & regression
Cfit = 0:0.1:7;
Tfit = 3:0.1:14;
[CFIT,TFIT] = meshgrid(Cfit,Tfit);
SRFIT = b(1) + b(2)*CFIT + b(3)*TFIT + b(4)*CFIT.*TFIT;

% Contour plot
v = min(min(SRFIT)):0.01:max(max(SRFIT));
figure, [c,h] = contourf(CFIT,TFIT,SRFIT,v);
title('\itSR_Z'), xlabel('C (%)'), ylabel('T (%)')
set(h,'EdgeColor','none');
colorbar;

% Overlay location of empirical TC data points
hold on
scatter(C,T,'*k')
```

Code used to generate frequency maps of cell location from gray-scale images of nuclei (Figure 5.2)

```
%% Stack, threshold, and visualize images
```

```
% Images to be stacked should all be in the same directory
% Images are treated as 2D arrays of unsigned 8-bit integers
% Create an array of filenames that make up the image sequence
fileFolder = fullfile('/Path/To/Images/');
dirOutput = dir(fullfile(fileFolder,'*.JPG'));
fileNames = {dirOutput.name}';
numFrames = numel(fileNames);

I = imread(fileNames{1});

% Preallocate first (grayscale, 8-bit) array
sequence = zeros([size(I(:,:,1)) numFrames],class(I));
% Set first 2D element in 'sequence' to the first read image
sequence = I(:,:,1);

% Read in images to the stack called 'sequence'
for p = 2:numFrames
    J = imread(fileNames{p});
    sequence(:,:,p) = J(:,:,1);
end

% Preallocate second (binary) array
b_sequence = zeros([size(I(:,:,1)) numFrames],class(I));
% Set first 2D element in b_sequence to the first thresholded image
b_sequence = thresh(sequence(:,:,1));

% Threshold images from 'sequence' using custom threshold function THRESH
for k = 2:numFrames
     b_sequence(:,:,k) = thresh(sequence(:,:,k));
end

% Sum binary frames along 3rd dimension, divide by # of frames to get freq
freq_sequence = sum(b_sequence,3)/numFrames;

% Plot
v = 0:0.05:1;
figure, [c,h] = contourf(freq_sequence,v);
set(h,'EdgeColor','none');
caxis([0 1]);
colorbar;
```

Thresholding function "thresh.m"

```
function [ binarized_image ] = thresh( image )
% Compute appropriate threshold value
level = graythresh(image);
% Use threshold value to binarize image
binarized_image = im2bw(image,level);
end
```

Contour plots of radial analysis

Although this script is not applied in this thesis, it has proven to be a useful tool for analysis in other projects, thus warranting its inclusion.

A radial analysis approach is used here to determine the degree of collagen alignment surrounding a cell in a confocal reflectance image of collagen. The script reads in an array of pixel intensity values as a function of distance and degrees measured in NIH ImageJ. The values are then shortened to the edge of the cell (by the "shorten" function) and intensities are plotted as distance vs. degrees. These plots reveal the morphology of collagen alignment and are useful for comparing images of cells in with aligned collagen where the differences are not immediately apparent.

Additionally, this technique can be adapted to plot the distance of the cell periphery from its centroid as a function of degrees. For example, observing the periphery at a consistent distance from the centroid across all degrees would indicate a circular morphology while two peaks separated by roughly 180 ° would indicate an elongated morphology. This provides a quantitative measure of cell morphology that could be used to describe more complex cell shapes.

Code used to analyze radial information to generate an average intensity plot and contour plot

```
%% Concatenate %%           % read in tab delimited data files from ImageJ
A = dlmread('Results0.xls', '', 1, 1);          % read in initial file
for i = 1:1:359                                 % iterate through all files
    filename = ['Results' num2str(i) '.xls'];   % read in next file
    I = dlmread(filename, '', 1, 1);
    A = cat(2, A, I);                           % add next file to matrix
end
dlmwrite('All.txt', A, '\t')  % write concatenated data to file
```

```
Shorten % See custom function Shorten.m below

%% Plot %%
A = dlmread('All_short.txt', '');   % read data
L = size(A);        % get size
r = 1:L(1,1);       % generate x values in pixels
pxum = 2.8;         % number of pixels in one micron (specific to image)
R = r/pxum;         % set X values in microns

% Generate plot values
Am = mean(A,2);         % average values over all rays
D = 0:359;              % generate degree index
Half = trapz(Am)/2;     % calculate half of area under the averaged curve
AmC = cumtrapz(Am);     % generate array of the cumulative sum of the average
BL = mean(Am(L(1,1)-10:L(1,1))); % determine baseline intensity from last 10 values
AmN = Am-BL;            % normalize averaged values to baseline
HalfN = trapz(AmN)/2;   % calculate half of area under the normalized average curve

% Determine the "mean" of the averaged curve as if it were a distribution
for i = 1:1:L(1,1)      % search along length
    if AmC(i) > Half    % until half of the area has been passed
        HalfLoc = i;    % remember location where half is passed
        break
    end
end
xmean = ['Distance (\mum), mean at ' num2str(R(i))];

% Determine the "mean" of the averaged curve (after normalization)
for j = 1:1:L(1,1)      % search along length
    if AmC(j) > HalfN   % until half of the area has been passed
        HalfLocN = j;   % remember location where half is passed
        break
    end
end
xmeanN = ['Distance (\mum), mean at ' num2str(R(j))];

% Plot parameters
IntensMin = 0;
IntensMax = 255;
% vector indicating contour lines should be every 15 units of intensity
v = IntensMin:1:IntensMax;

% Plot averaged data over all rays
figure, subplot(2,1,1), plot(R,Am)
xlabel(xmean), ylabel('Intensity (a.u.)'), axis([0 22 IntensMin IntensMax])

% Plot normalized averaged data over all rays
subplot(2,1,2), plot(R,AmN)
xlabel(xmeanN), ylabel('Intensity (a.u)'), axis([0 22 IntensMin IntensMax])

% Contour Plot over all rays
figure, [c,h] = contourf(D,R,A,v);
xlabel('Angle (degrees)'), ylabel('Distance (\mum)')
set(h,'EdgeColor','none');
```

```
colorbar;
```

Custom function ”Shorten.m”

```
A = dlmread('All.txt', '', 0, 0);   % read data from file
S = size(A);                        % get size of data set

% shift rays so that non-zero values start at position 1
for k = 1:1:S(1,2)          % iterate for all rays
j = 1;
    for i = 1:1:S(1,1);     % iterate through the entire length of ray
        if A(i,k) > 0;      % if element i is non-zero
            A(j,k) = A(i,k);% place it at position j
            A(i,k) = 0;     % and set position i to zero
            j = j + 1;      % increment position j
        end
    end
end

% shorten matrix height to that of shortest column
for m = 1:1:S(1,1)              % iterate through all degrees
    for k = 1:1:S(1,2)          % iterate through all rays
        if A(m,k) == 0          % if element is zero
            for j = S(1,1):-1:m % delete end row up to the current row
                A(j,:) = [];
            end
            dlmwrite('All_short.txt', A, '\t'); % write data to a new file
            return
        end
    end
end
```

REFERENCES

[1] Charest JM, Califano JP, Carey SP, Reinhart-King CA (in press) Fabrication of Substrates with Defined Mechanical Properties and Topographical Features for the Study of Cell Migration. *Macromolecular Bioscience*.

[2] Nelson CM, Inman JL, Bissell MJ (2008) Three-dimensional lithographically defined organotypic tissue arrays for quantitative analysis of morphogenesis and neoplastic progression. *Nature Protocols* 3:674–678.

[3] Carey SP, Charest JM, Reinhart-King CA (2011) *Forces During Cell Adhesion and Spreading*, Studies in Mechanobiology, Tissue Engineering and Biomaterials, ed Gefin A (Springer) Vol. 4, 1 edition.

[4] Carmeliet P (2003) Angiogenesis in health and disease. *Nature Medicine* 9:653–660.

[5] Herbert SP, Stainier DYR (2011) Molecular control of endothelial cell behaviour during blood vessel morphogenesis. *Nature Reviews Molecular Cell Biology* 12:551–564.

[6] Ingber DE (2002) Mechanical signaling and the cellular response to extracellular matrix in angiogenesis and cardiovascular physiology. *Circulation Research* 91:877–887.

[7] Ingber DE, Folkman J (1989) Mechanochemical switching between growth and differentiation during fibroblast growth factor-stimulated angiogenesis in vitro: role of extracellular matrix. *The Journal of Cell Biology* 109:317–330.

[8] Paszek MJ, et al. (2005) Tensional homeostasis and the malignant phenotype. *Cancer Cell* 8:241–254.

[9] Zwerger M, Ho CY, Lammerding J (2011) Nuclear mechanics in disease. *Annual Review of Biomedical Engineering* 13:397–428.

[10] Buxboim A, Ivanovska I (2010) Matrix elasticity, cytoskeletal forces and physics of the nucleus: how deeply do cells 'feel' outside and in? *Journal of Cell Science* 123:297–308.

[11] Biela SA, Su Y, Spatz JP, Kemkemer R (2009) Different sensitivity of human

endothelial cells, smooth muscle cells and fibroblasts to topography in the nano-micro range. *Acta Biomaterialia* 5:2460–2466.

[12] Pelham RJ, Wang YL (1997) Cell locomotion and focal adhesions are regulated by substrate flexibility. *Proceedings of the National Academy of Sciences* 94:13661–13665.

[13] Lo CM, Wang HB, Dembo M, Wang YL (2000) Cell movement is guided by the rigidity of the substrate. *Biophysical Journal* 79:144–152.

[14] Peyton SR, Putnam AJ (2005) Extracellular matrix rigidity governs smooth muscle cell motility in a biphasic fashion. *Journal of Cellular Physiology* 204:198–209.

[15] Yeung T, et al. (2005) Effects of substrate stiffness on cell morphology, cytoskeletal structure, and adhesion. *Cell Motility and the Cytoskeleton* 60:24–34.

[16] Califano JP, Reinhart-King CA (2008) A Balance of Substrate Mechanics and Matrix Chemistry Regulates Endothelial Cell Network Assembly. *Cellular and Molecular Bioengineering* 1:122–132.

[17] Reinhart-King CA, Dembo M, Hammer DA (2005) The dynamics and mechanics of endothelial cell spreading. *Biophysical Journal* 89:676–689.

[18] Wang H, Dembo M (2000) Substrate flexibility regulates growth and apoptosis of normal but not transformed cells. *The American Journal of Physiology: Cell Physiology* 279:C1345–C1350.

[19] Wang Y, Wang G, Luo X, Qiu J, Tang C (2011) Substrate stiffness regulates the proliferation, migration, and differentiation of epidermal cells. *Burns*.

[20] Engler AJ, Sen S, Sweeney HL, Discher DE (2006) Matrix elasticity directs stem cell lineage specification. *Cell* 126:677–689.

[21] Reinhart-King CA (2011) How matrix properties control the self-assembly and maintenance of tissues. *Annals of Biomedical Engineering* 39:1849–1856.

[22] Curtis AS, Wilkinson CD (1997) Topographical control of cells. *Biomaterials* 18:1573–1583.

[23] Curtis AS, Wilkinson CD (1998) Reactions of cells to topography. *Journal of Biomaterials Science Polymer Edition* 9:1313–1329.

[24] Bettinger CJ, Langer R, Borenstein JT (2009) Engineering Substrate Topography at the Micro- and Nanoscale to Control Cell Function. *Angewandte Chemie International Edition* 48:5406–5415.

[25] Dalby MJ, et al. (2007) The control of human mesenchymal cell differentiation using nanoscale symmetry and disorder. *Nature Materials* 6:997–1003.

[26] Biggs MJP, et al. (2008) Adhesion formation of primary human osteoblasts and the functional response of mesenchymal stem cells to 330nm deep microgrooves. *Journal of the Royal Society, Interface* 5:1231–1242.

[27] Biggs MJP, et al. (2009) The use of nanoscale topography to modulate the dynamics of adhesion formation in primary osteoblasts and ERK/MAPK signalling in STRO-1+ enriched skeletal stem cells. *Biomaterials* 30:5094–5103.

[28] Biggs MJP, et al. (2009) Interactions with nanoscale topography: adhesion quantification and signal transduction in cells of osteogenic and multipotent lineage. *Journal of Biomedical Materials Research Part A* 91:195–208.

[29] Kulangara K, Leong KW (2009) Substrate topography shapes cell function. *Soft Matter* 5:4072–4076.

[30] Teixeira AI, Abrams GA, Bertics PJ, Murphy CJ, Nealey PF (2003) Epithelial contact guidance on well-defined micro- and nanostructured substrates. *Journal of Cell Science* 116:1881–1892.

[31] Chrambach A, Rodbard D (1971) Polyacrylamide gel electrophoresis. *Science* 172:440–451.

[32] Wang YL, Pelham RJ (1998) Preparation of a flexible, porous polyacrylamide substrate for mechanical studies of cultured cells. *Methods in Enzymology* 298:489–496.

[33] Pless DD, Lee YC, Roseman S, Schnaar RL (1983) Specific cell adhesion to immobilized glycoproteins demonstrated using new reagents for protein and glycoprotien immobilization. *The Journal of Biological Chemistry* 258:2340–2349.

[34] Beningo K, Lo C, Wang Y (2002) Methods in Cell Biology: Flexible polyacrylamide substrata for the analysis of mechanical interactions at cell-substratum adhesions. *Methods in Cell Biology*.

[35] Boudou T, Ohayon J, Picart C, Pettigrew RI, Tracqui P (2009) Nonlinear elastic properties of polyacrylamide gels: implications for quantification of cellular forces. *Biorheology* 46:191–205.

[36] Basu A, et al. (2011) Nonaffine Displacements in Flexible Polymer Networks. *Macromolecules* 44:1671–1679.

[37] Lemmon CA, et al. (2005) Shear force at the cell-matrix interface: enhanced analysis for microfabricated post array detectors. *Mechanics & Chemistry of Biosystems* 2:1–16.

[38] Patel S, Rodriguez F, Cohen C (1989) Mechanical and Swelling Properties of Polyacrylamide-Gel Spheres. *Polymer* 30:2198–2203.

[39] Richards EG, Temple C (1971) Some Properties of Polyacrylamide Gels. *Nature Physical Science* 230:92–96.

[40] Rüchel R, Steere R, Erbe E (1978) Transmission-Electron Microscopic Observations of Freeze-Etched Polyacrylamide Gels. *Journal of Chromatography* 166:563–575.

[41] Stellwagen NC (1998) Apparent pore size of polyacrylamide gels: comparison of gels cast and run in Tris-acetate-EDTA and Tris-borate-EDTA buffers. *Electrophoresis* 19:1542–1547.

[42] Lira LM, Martins KA, Cordoba de Torresi SI (2009) Structural parameters of polyacrylamide hydrogels obtained by the Equilibrium Swelling Theory. *European Polymer Journal* 45:1232–1238.

[43] Flory P, Rehner J (1943) Statistical mechanics of cross-linked polymer networks II Swelling. *Journal of Chemical Physics* 11:521–526.

[44] Boyde T (1976) Swelling and Contraction of Polyacrylamide-Gel Slabs in Aqueous-Solutions. *Journal of Chromatography* 124:219–230.

[45] Weiss P (1958) *International Review of Cytology*, International Review of Cytology (Elsevier) Vol. 7.

[46] Buck RC (1979) Contact guidance in the subendothelial space. Repair of rat aorta in vitro. *Experimental and Molecular Pathology* 31:275–283.

[47] Poellmann MJ, Harrell PA, King WP, Johnson AJW (2010) Geometric microenvironment directs cell morphology on topographically patterned hydrogel substrates. *Acta Biomaterialia* 6:3514–3523.

[48] Liu L, et al. (2011) Probing the invasiveness of prostate cancer cells in a 3D microfabricated landscape. *Proceedings of the National Academy of Sciences* 108:6853–6856.

[49] Parker K, et al. (2002) Directional control of lamellipodia extension by constraining cell shape and orienting cell tractional forces. *The FASEB Journal* 16:1195–1204.

[50] Wang N, Ostuni E, Whitesides GM, Ingber DE (2002) Micropatterning tractional forces in living cells. *Cell Motility and the Cytoskeleton* 52:97–106.

[51] Rape AD, Guo WH, Wang YL (2011) The regulation of traction force in relation to cell shape and focal adhesions. *Biomaterials* 32:2043–2051.

[52] Buxboim A, Discher DE (2010) Stem cells feel the difference. *Nature Methods* 7:695–697.

[53] Fu J, et al. (2010) Mechanical regulation of cell function with geometrically modulated elastomeric substrates. *Nature Methods* 7:733–736.

[54] Flanagan LA, Ju YE, Marg B, Osterfield M, Janmey PA (2002) Neurite branching on deformable substrates. *Neuroreport* 13:2411–2415.

[55] Roy R, Boskey AL, Bonassar LJ (2008) Non-enzymatic glycation of chondrocyte-seeded collagen gels for cartilage tissue engineering. *Journal of Orthopaedic Research* 26:1434–1439.

[56] Roy R, Boskey AL, Bonassar LJ (2010) Processing of type I collagen gels using nonenzymatic glycation. *Journal of Biomedical Materials Research Part A* 93:843–851.

[57] Nelson CM, Vanduijn MM, Inman JL, Fletcher DA, Bissell MJ (2006) Tissue geometry determines sites of mammary branching morphogenesis in organotypic cultures. *Science* 314:298–300.

[58] Mori H, Gjorevski N, Inman JL, Bissell MJ, Nelson CM (2009) Self-organization of engineered epithelial tubules by differential cellular motility. *Proceedings of the National Academy of Sciences* 106:14890–14895.

[59] Gomez EW, Chen QK, Gjorevski N, Nelson CM (2010) Tissue geometry patterns epithelial-mesenchymal transition via intercellular mechanotransduction. *Journal of Cellular Biochemistry* 110:44–51.

[60] Gjorevski N, Nelson CM (2010) Endogenous patterns of mechanical stress are required for branching morphogenesis. *Integrative Biology* 2:424–434.

[61] Gomez EW, Nelson CM (2011) Lithographically defined two- and three-dimensional tissue microarrays. *Methods in Molecular Biology* 671:107–116.